IEEE Access
Multidisciplinary ⋮ Rapid Review ⋮ Open Access Journal

Received June 6, 2021, accepted June 27, 2021, date of publication July 1, 2021, date of current version July 9, 2021.

Digital Object Identifier 10.1109/ACCESS.2021.3093856

Experimental Evaluation of Aerial Manipulation Robot in Contact With 15 kV Power Line: Shielded and Long Reach Configurations

ALEJANDRO SUAREZ[1], RAFAEL SALMORAL[1], PEDRO J. ZARCO-PERIÑAN[2], AND ANIBAL OLLERO[1], (Fellow, IEEE)

[1]GRVC Robotics Laboratory, School of Engineers, University of Seville, 41092 Seville, Spain
[2]Department of Electrical Engineering, School of Engineers, University of Seville, 41092 Seville, Spain

Corresponding author: Alejandro Suarez (asuarezfm@us.es)

This work was supported in part by the AERIAL COgnitive integrated multi-task Robotic system with Extended operation range and safety (AERIAL-CORE) Project of the European Commission under Grant H2020-2019-871479, and in part by the European Research Council Advanced Grant General compliant aerial Robotic manipulation system Integrating Fixed and Flapping wings to INcrease range and safety (GRIFFIN) under Grant 788247.

ABSTRACT The use of aerial manipulators for the inspection and maintenance of the power grid requires the safe interaction of the robot with high voltage power lines. In order to identify possible faults or malfunctions during the approaching or interaction phases, this paper presents experimental results in a real 15 kV power line, considering four different configurations for the manipulator: 1) aluminum tube attached to the landing gear, 2) robotic arm attached to the multi-rotor base, 3) shielded aerial manipulator, and 4) long reach configuration (insulated). The paper investigates the electromagnetic susceptibility of the autopilot and the electronic speed controllers to the electrostatic discharge (ESD) raised when the manipulator touches the line, causing the momentary failure of the rotors. A model of the electromagnetic effects associated to the interaction with the line is provided, comparing later the effectiveness of the two solutions for the aerial manipulator: shielding, and insulation.

INDEX TERMS Aerial manipulation, power lines, electrostatic discharge.

I. INTRODUCTION

The inspection and maintenance of power lines represents a significant economic cost for the supply companies due to the vast extension of this kind of infrastructure and the need to perform these tasks periodically according to the regulation of each country or region. Not only that, but the high altitude of the transmission lines requires the deployment of the operators through heavy vehicles like elevated work platforms or even manned helicopters, becoming a complex problem depending on the available access routes by land. Note for example that Spain, a medium size country, has almost 300.000 km of high/medium voltage overhead lines [1]. The installation of devices like bird flight diverters, electrical spacers, vibration dampers, or anti-nests illustrated in Figure 1 is a common operation carried out by human operators on live power lines, with the consequent risk due to the high altitude and high voltage of the lines [2].

The associate editor coordinating the review of this manuscript and approving it for publication was Mohammad Alshabi.

The recent advances in the development and application of the aerial manipulation technology [3]–[5] in representative outdoor scenarios like chemical plants [6] or bridges [7], and the wide variety of operations that can be conducted with an aerial manipulator [8]–[12], has motivated the interest in employing this kind of robots for the installation of devices as well as for the maintenance of power lines [13] with the aim to reduce the time, cost, and risk w.r.t. (with respect to) conventional solutions carried out by human workers [2]. The technological challenges are still considerable. First of all, the effect of the electromagnetic interference (EMI) generated by the high voltage power line over the inertial measurement unit (IMU), GNSS (global navigation satellite system) sensors, and other electronic components embedded on the aerial platforms has not been properly documented [14]. Reference [15] analyzes the Corona discharge on a quadrotor within an offshore HVDC wind farm, whereas [16], [17] consider the electrostatic fields produced by a power line on a manned helicopter. Second, the installation of devices like bird flight diverters, electrical spacers, vibration dampers,

shown in Figure 1, requires a significant level of dexterity, especially in the helical diverter and in the spacers. In this sense, the use of dual arm aerial manipulators [8], [18] allows the replication of the bimanual manipulation capabilities of the human operators. Also, the long reach configuration [8] increases the separation distance between the propellers and the cables, and with it, the safety. Third, given the number of devices to be installed on a single section between two poles (what may vary between 10 and 50), and taking into account the limited payload capacity of the multi-rotor platforms, it is highly desirable to optimize the time performance of the operation [19], [20].

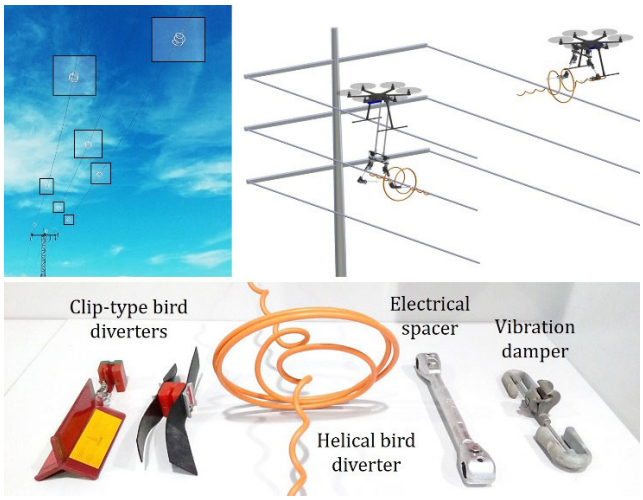

FIGURE 1. Helical bird flight diverters (up-left) installed by dual arm aerial manipulators (up-right) along with other devices typically installed on the power lines (down).

The literature review in power line inspection robots and techniques [21], [22] reveals a wide diversity of technological solutions intended to perform the inspection operation with the possibility to avoid the obstacles along the line, including insulators, jumpers, suspension towers, as well as the devices shown in Figure 1. Three categories of robots are identified according to the locomotion method: climbing, flying, and hybrid flying-climbing. The first group comprises dual arm and multi-arm systems capable of rolling along the lines and bypassing obstacles. The use of aerial platforms, either heli-copters [23] or multirotors [24], is focused on the inspection of the power lines employing visual, thermal or infrared cameras for detecting faults or damaged components. Multi-rotors are nowadays extensively used due to their higher maneuverability and controllability compared to helicopters. Although climbing-rolling robots provide longer operation times than aerial robots, the difficulty in their deployment or retrieval from the power line (especially taking into account their weight, that may vary from 10 up to 100 kg [21]) is considerable, whereas the ability of VTOL (vertical take-off and landing) UAVs (unmanned aerial robots) like multi-rotors, whose weight is typically under 10 kg, reduces significantly the time required to reach the points of interest. Hybrid solutions as the one presented in [14] aim to extend the operation time by incorporating a rolling mechanism that allows the robot to move along the line with lower energy consumption after landing on it.

Unlike the visual inspection operations conducted with manned helicopters [16], [17] and unmanned aerial platforms [14], [15], [21]–[24] by flying several meters away from the power lines, the realization of maintenance tasks like the installation of bird flight diverters using aerial manipulation robots as illustrated in Figure 1 involves the physical and electromagnetic interaction with the conductors in a closer range, raising two problems: the accurate positioning of the aerial robot with respect to the power line, and the electrical protection of the onboard electronic components. Regarding the first point, reference [25] exploits the magnetic field generated by the electric current flowing through the line for estimating the location of the aerial platform, whereas reference [26] proposes the use of a dual arm aerial manipulator for position estimation and force control relative to a grabbing point fixed to the power line. On the other hand, although some solutions for the installation of clip-type bird diverters employing commercial drones have been recently demonstrated [27], [28], the study of the possible effects and malfunctions on aerial manipulators caused by high voltage live power lines is still missing. Reference [15] reports preliminary results and simulations on high electrostatic field applied to a multi-rotor in laboratory conditions without flying, employing later a X-shaped aluminum frame that models the drone body to evaluate the effect of shielding on the corona discharge. The prototype shown in [14] also incorporates metallic shielding cages to protect the onboard components from the electrical interferences, what increases the weight of the drone (14 kg). However, the design of the shield is not documented.

The main contribution of this paper is the experimental evaluation of an aerial manipulation robot interacting with a 15 kV live power line, identifying some malfunctions of the onboard components due to the electromagnetic interference generated by the high voltage and the electrostatic discharge (ESD) raised when the manipulator touches the line. The paper analyzes and models these effects from the literature review, proposing four different configurations of manipulate-tors whose effectiveness is compared. These are: 1) simple aluminum tube attached to the landing gear, 2) robotic arm attached to multirotor base, 3) shielded aerial manipulator, and 4) long reach aerial manipulator (insulated).

The rest of the paper is organized as follows. Section II describes the platform and preliminary flight tests carried out on a 15 kV live power line, identifying the fault in one of the tests. Section III analyzes the causes of the fault and develops a model of the system and the environmental conditions that will be used in Section IV for the design of the shielded and insulated aerial manipulators. Section V compares the results of the different experiments presented in the paper, whereas Section VI summarizes the conclusions of this work.

II. PRELIMINARY FLIGHT TESTS

A. CONSIDERATIONS IN THE DESIGN OF THE TESTS

The installation of the devices depicted in Figure 1 using an aerial manipulation robot involves the physical contact with a live power line at high electric potential. Besides the electro-magnetic field generated by the line, the potential difference between this and the aerial robot will cause an unpredictable effect in the on-board components (autopilot, electronic speed controllers, brushless motors, servos, computer boards) during the transition from contactless to contact. The preliminary flight tests described in this section are intended to identify the possible malfunctions in the aerial robot when approaching or interacting with a real power line, as depicted in Figure 2.

FIGURE 2. Aerial manipulation robot approaching to a 15 kV power line.

Due to the uncertainty in the behavior of the aerial platform in its interaction with the live power line, and considering that an electric/electronic failure on the on-board components will probably cause the crash of the platform, the experiments were designed as a sequence of tests with increasing level of risk. These are indicated in Table 1. The execution of the four tests can be seen in the video attachment [29]. However, the paper is focused on analyzing the effects identified in tests 2, 3 and 4 since no significant effects were observed in test 1, although this is included in the video attachment [29].

TABLE 1. Sequence of experiments for approaching and interacting with the power line, from lower to higher risk of fault.

Test	Goal	Configuration
1	Approach from below to the power line to detect interferences on IMU or in the electronic components.	Attitude control mode (no GPS). No physical contact with the power line.
2	Touch the power line with a 60 cm length aluminum tube attached to the leg of the landing gear.	Attitude control mode (no GPS), anodized aluminum tube used as manipulator.
3	Touch the power line with a 60 cm length aluminum tube attached to the leg of the landing gear.	Position control with GPS, anodized aluminum tube used as manipulator.
4	Touch the power line with a 50 cm reach, 2-DOF robotic arm built with conventional servo actuators.	Position control with GPS. Manipulator built in aluminum structure, attached to multirotor base.

B. AERIAL PLATFORM

In order to make the experiments reproducible, this section describes in detail the platform employed in the preliminary flight tests, remarking the differences in the setup of tests 2-3 and 4, since the identified failure occurs in the latter.

The aerial platform consists of a S550 hexarotor, similar to the DJI F550, equipped with six DJI 2312E brushless motors, DJI 430 LITE electronic speed controllers (ESC), and 9 × 4.5" propellers. The autopilot is a Pixhawk with PX4 v.1.11.3, fed by its power module connected to the multirotor battery (4S 4400 mAh), integrating a Futaba R6303SB radio receiver and a 3DR GPS. These components were selected since they are widely used in several research works. For test 4, the platform incorporates a 2-DOF robotic manipulator built with Herkulex DRS-0402/0602 servos connected to the Raspberry Pi model 3B+ computer board where the control program is executed through a FTDI USART interface, and a 5V USB battery. The components are represented in Figure 3 along with the electric connections, indicating possible interference points due to inductive or capacitive coupling with the EMI source [30].

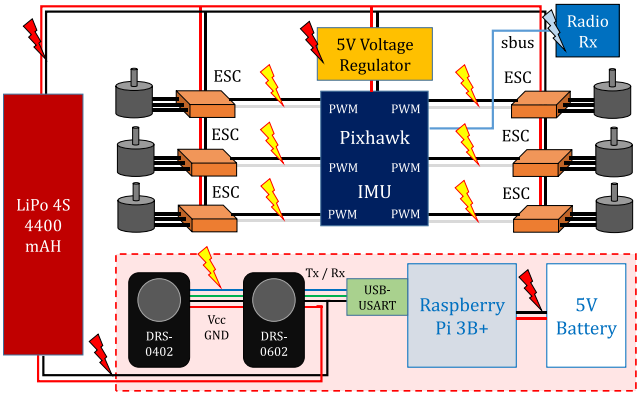

FIGURE 3. Components and connections of the aerial robot used in the tests. The components within the pink-shaded area correspond to the manipulator (only in test 4). The color rays represent possible EMI on the power cables (red), on the PWM/USART signals (yellow) and in the radio signal (blue).

The two types of manipulators integrated in the platform for experiments 2-3 and 4 are depicted in Figure 4. The first one is a simple anodized aluminum tube, 600 mm length 6 mm Ø, attached to the leg of the landing gear with zip ties. The second one is the 2-DOF robotic arm attached to the multirotor base (under the autopilot), connected to the Raspberry Pi and powered by the 4S LiPo battery of the multirotor.

C. FIRST CONTACT TESTS WITH ALUMINUM TUBE

The goal of tests 2 and 3 is to identify possible failures or any malfunction in the aerial platform due to the interaction with the 15 kV power line. The procedure of both experiments is the same: the platform takes-off, approaches from above to the higher phase of the tower until the aluminum tube touches the cable, and flies back to the landing point.

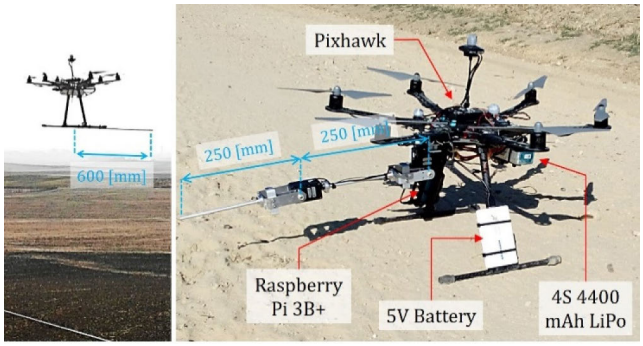

FIGURE 4. Aerial manipulation robot with aluminum tube attached to the leg of the landing gear (left) and 2-DOF robotic arm (right) used in test 4.

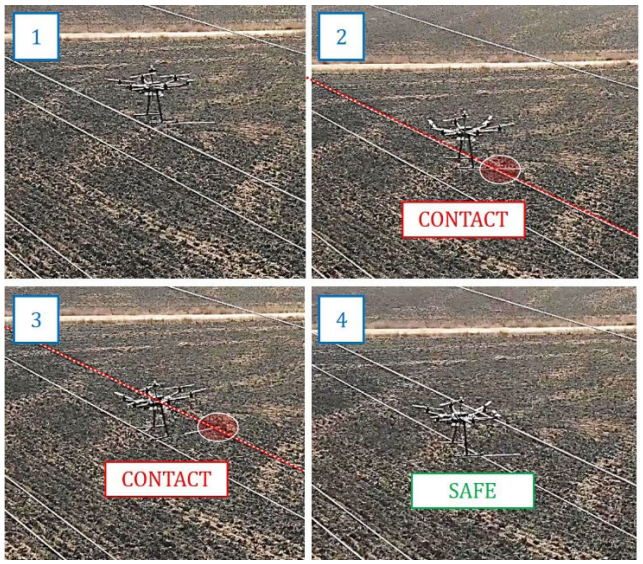

FIGURE 5. Hexarotor touching the 15 kV power line with a 600 mm length, 6 mm Ø anodized aluminum tube attached to the landing gear.

The multirotor was controlled in attitude mode (test 2) and GPS position mode (test 3) by an expert human pilot. The visual inspection of the video attachment [29] and the image sequence shown in Figure 5 reveal that the platform is not significantly affected by the power line, although the analysis of the data log given by the autopilot shows that the noise in the magnetometer increases considerably as the robot is closer to the power line (Figure 6). When the manipulator touches the cable, the norm of the noise exceeds the strength of the Earth's magnetic field (0.4 Gauss). Note that the brushless motors of the propellers or the DC motors of the servos are not significantly affected since the magnetic field of their magnets is in the range of 1 T (10.000 Gauss).

D. FIRST CONTACT TEST WITH ROBOTIC ARM

The experiment was repeated replacing the aluminum tube by the 2-DOF robotic arm, integrating also the Raspberry Pi 3B+ and the 5V battery as indicated in Figure 3 and Figure 4. The multirotor was controlled in GPS position mode, following a trajectory similar to previous tests to approach

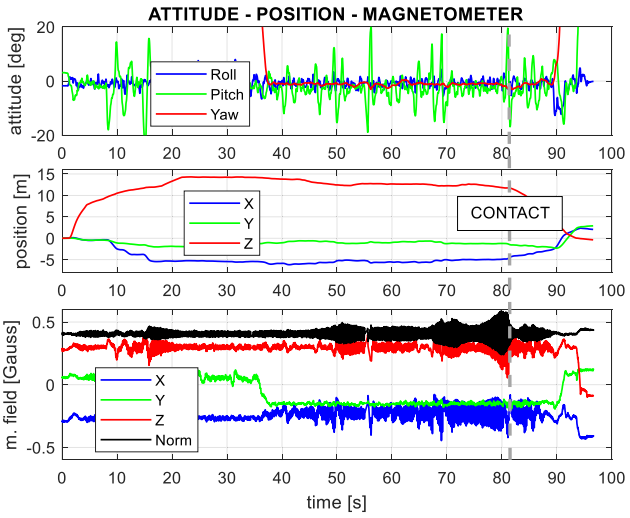

FIGURE 6. Multirotor attitude, position, and magnetic field measured by the IMU in test 3. The amplitude of the noise increases in the XZ axes as the platform approaches to the power line, although this does not affect significantly the attitude estimation and control. The contact with the line occurs at the =81 s.

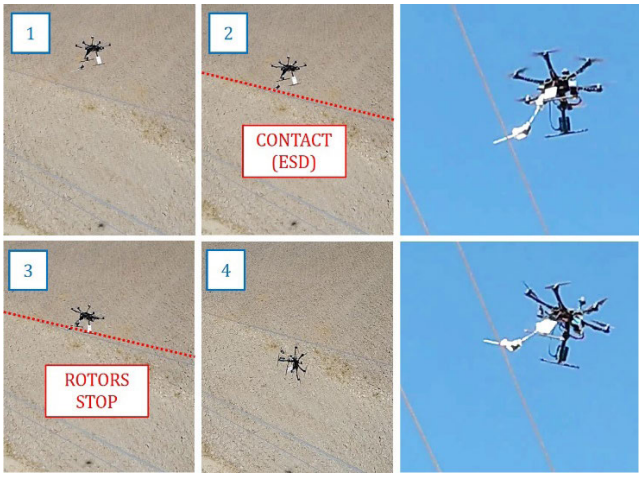

FIGURE 7. Hexarotor platform touching the 15 kV power line with the forearm link (anodized aluminum) of the 2-DOF robotic arm attached to the base. The propellers stop when the contact occurs, crashing due to the propeller lost.

the power line. However, in this case, the contact of the forearm link of the manipulator with the power line caused a sudden stop of the propellers. The video of the experiment [29] evidences that the fault occurs exactly when the arm touches the power line (at 10 cm from the elbow servo, approximately) and that the aerial platform tries to recover the control before the crash, although the velocity in the free fall was too high to be recovered. The strong deceleration of the motors caused by the active brake of the ESC also made that one of the propellers was unscrewed. The analysis of the data provided by the auto-pilot reveals that the log was interrupted at the same instant the fault occurs. As it will be seen in Section III-B, this fault was caused by the electrostatic discharge (ESD) due to the voltage difference.

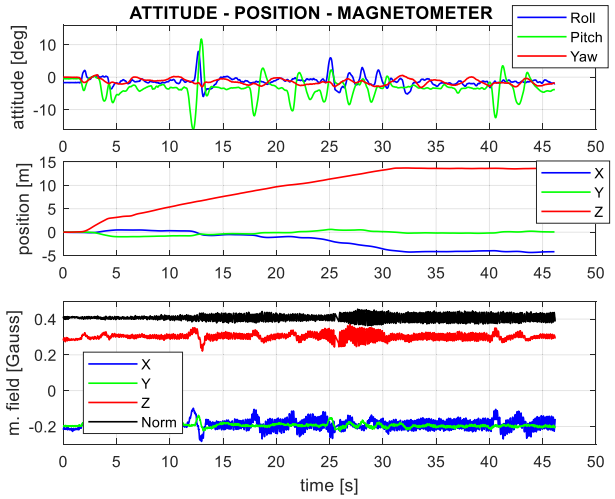

FIGURE 8. **Multirotor attitude, position, and magnetic field measured by the IMU in test 4. The amplitude of the noise is lower compared to test 3 when the arm interacts with the line at t = 46 s, when the fault occurs and log stops.**

It is interesting to note however that the amplitude of the noise in the magnetometer was lower in this case w.r.t. tests 2-3, as the distance between the power line and the IMU is higher when the robotic arm touches the cable (see Fig. 7 and Fig. 8).

III. FAULT ANALYSIS AND SYSTEM MODELING

A. FAULT ASSESMENT

Despite the failure and consequent crash occurred in test 4 when the arm touches the power line, no electronic component was damaged. It is necessary to remark that the autopilot tried to recover the control of the platform one or two seconds after the failure occurs, which rules out a power outage, as the autopilot usually takes around 10 s to boot. This suggests that the autopilot and/or the ESC were momentarily affected by the electrostatic discharge generated when the forearm link of the 2-DOF manipulator touches the power line. Unlike tests 2 and 3, in which the anodized aluminum tube is not electrically connected to the on-board components, the cable of the elbow servo (Figure 3) facilitated the propagation of the electrostatic discharge to the rest of components through the conductors [30]–[32] as the GND and VDD pins of the servos are con-nested to the LiPo battery that feeds the multirotor.

As it can be seen in the video attachment [29], the six rotors stop suddenly when the arm touches the power line, so the fault is common to the six speed controllers. The strong deceleration of the propellers is due to the active brake of the DJI 430 LITE ESC, which even caused that one of the blades was unscrewed. In order to investigate this fault, three tests were conducted to evaluate the behavior of the DJI 430 LITE ESC, injecting a PWM (pulse width modulation) signal at 50 Hz with the usual duty cycle in the range 1 – 2 ms (0 – 100 %). The ESC controls a DJI 2312E brushless motor, removing the propeller for safety reasons. In the test the motor is initially accelerated increasing the PWM from 0 to 30% in 2 seconds, maintaining the constant speed two additional seconds. Then, the fault is injected until the active brake is triggered, identifying three possible causes:

1) PWM pulse out of range (duty cycle $>$ 120% $\equiv$ 2.2 ms) for a single period (20 ms), which corresponds to a voltage peak in the PWM signal due to the ESD.
2) Four consecutive pulses with 0% PWM (duty cycle $=$ 1 ms). The ESC maintained the 30% speed for 70 ms, then the active brake was triggered.
3) PWM voltage signal down, which enables the pull-up resistor of the ESC and with it, the saturation of the signal (duty cycle $=$ 20 ms).

The momentary interruption of the microcontroller integral-ted in the autopilot and the ESC corresponds to behavior class B (failure detected but self-recovery after disturbance) or class C (external user action to recover normal functionality) according to the EMC (electromagnetic compatibility) design guide provided by the microcontroller's manufacturer [30]. This classification is related with the severity levels (1, 2, 3, 4) defined in norm IEC 61000-4-2 that correspond to voltages of $\pm$2, $\pm$4, $\pm$6, and $\pm$8 kV applied to the device under test (DUT).

Since the observed fault is due to the electrical interaction of the aerial robot with the power line, next subsections present some principles to facilitate the understanding of its causes and the possible solutions.

B. PRINCIPLES OF THREE PHASE ELECTRIC POWER

In order to facilitate the understanding of next subsection, it is convenient to review briefly the generation of three-phase electric power. Traditionally, most of the existing power grid employs AC (alternate current) for long distance transmission due to its higher efficiency compared to the DC (direct current) systems. The AC power generator transforms the mechanical energy from a turbine into electric energy through the current induced by a rotating magnetic field into the three coils of the generator. Figure 9 represents the electric diagram of the two configurations of the generator (star and delta), indicating the voltage/current on the lines and on the phase, which are 120° out of phase. The distribution line illustrated in Figure 2 has a nominal voltage of 15 kV (RMS line voltage), with a nominal current around 175 A at 50 Hz in delta connection.

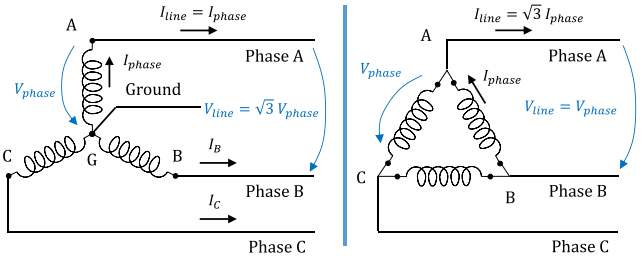

FIGURE 9. **Three-phase power generation: star (left) and delta (right) setups.**

C. ELECTRICAL INTERACTION MODEL

The study on the electrical interactions between the aerial manipulator and the transmission line can be approached from previous works analyzing the voltages and currents induced on conductors [33], humans [17], [34] or insulated objects [35], as is the case of the aerial manipulator. The goal now is to derive a model that describes qualitatively these interactions and their relevant effects, taking into account that it is not feasible to model electrically the robot due to the complex distribution of all the conductors and the insulation materials employed on its construction. In order to provide analytical solutions, many works consider simple spherical models [36], [37] or simplified geometries [16]. Electromagnetic field simulation software like Ansys Maxwell has been also employed in [16] to study the perturbation in the electric field generated by a power line due to the proximity of a helicopter model, comparing the field measurements with simulation results. Although the current that flows through the power line corresponds to a time varying linear distribution of charge, the relatively slow time rates (50/60 Hz) and the small size of the aerial robot compared to the wavelengths allows to conduct an electrostatic analysis.

The aerial robot (AR) approaching to the power line (PL) can be assimilated to a floating conductor [36] represented by a sphere characterized by its electric potential V_{AR} and charge Q_{AR}, being both zero when the platform is landed/grounded. As stated in [36], a conductor with an arbitrary geometry can be approximated by a sphere with the same surface. The power line will be also assimilated in the first place to a sphere at potential V_{PL} and charge Q_{PL} to describe the electrical relation between both bodies, given by Maxwell's equations:

$$Q_{AR} = C_{AR}V_{AR} + C_{AR}^{PL}V_{PL} \tag{1}$$

$$Q_{PL} = C_{AR}^{PL}V_{AR} + C_{PL}V_{PL} \tag{2}$$

Here $C_{AR} = 4\pi\varepsilon_0 R$ is the self-capacitance of the equivalent sphere of radius R that models the aerial robot [34], ε_0 is the vacuum permittivity, whereas C_{AR}^{PL} is the mutual capacitance between the aerial robot and the section of power line that interacts with the robot. The second term on the right side of Equation (1) indicates that the aerial robot is charged while it approaches to the potential of the line due to the capacitive coupling, resulting on the following potential:

$$V_{AR} = \frac{Q_{AR} - Q_{PL}\left(C_{AR}^{PL}/C_{AR}\right)}{C_{PL} - \left(C_{AR}^{PL}\right)^2/C_{AR}} \tag{3}$$

This is relevant in terms of safety, as the aerial robot should be discharged before it is touched by a human operator [34], especially if the metallic surface of the robot is significant. The electrostatic discharge event occurs when the electric field strength E caused by the potential difference ΔV between the two bodies, separated a distance d, exceeds the breakdown strength of dielectric medium (the air), $E_b^{air} = 3kV/mm$:

$$E = k\frac{\Delta V}{d} = k\frac{V_{PL} - V_{AR}}{d} \geq E_b^{air} \tag{4}$$

where k is a scale factor that depends on the configuration of the bodies [37] ($k = 1$ for parallel plates). As shown in [16], the distortion of the electrostatic field is more pronounced for geometries with high curvatures, typically in the corners or edges of the frame structure of the robot, or in the propellers. For the 15 kV power line, the ESD event will occur when the separation distance d is below 5 cm [2] (see Section IV-A).

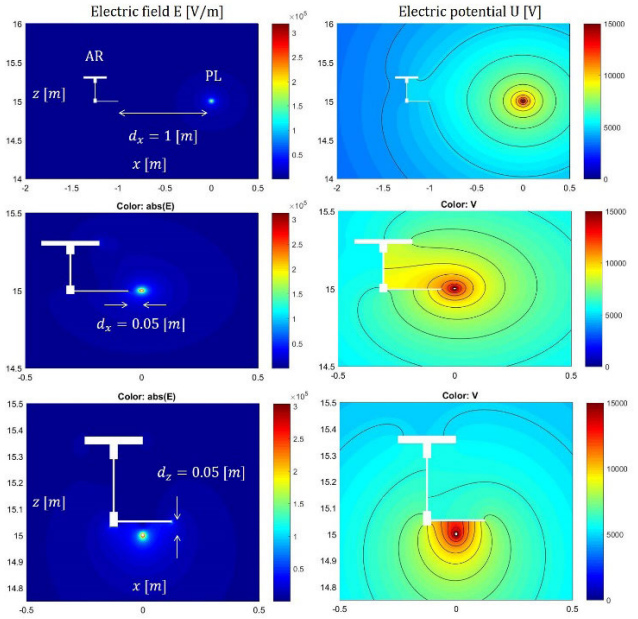

FIGURE 10. Electric field (left) and potential (right) when the aerial robot (AR) at floating potential approaches to the 15 kV power line (PL) along the XZ-axes. The equipotential lines are drawn for increments of 1000 V.

The distribution of the electric field and electric potential of a simplified 2D geometry of the aerial robot approaching to the power line, showed in Figure 10, is obtained in simulation using the PDE toolbox of MATLAB. This can be formulated as an electrostatics problem, consisting of solving the Poisson equation derived from the Maxwell's equations:

$$-\nabla \cdot (\varepsilon \nabla V) = \rho; \quad \boldsymbol{E} = \nabla V \tag{5}$$

where $\boldsymbol{E}$ and V are the electric field vector and potential, respectively, ε is the dielectric permittivity of the environment, whereas ρ is the space charge density. In the simulation, the power line is located at 15 m height within a 20 m width by 30 m height free space characterized by its dielectric permittivity ε_0 and zero space charge density. Three boundary conditions are imposed in this system: (1) zero potential in the contour of the free space; (2) 15 kV potential in the contour of the power line; (3) zero surface charge on the aerial robot. Note that this simulation is conducted on the XZ plane. Advanced software like Ansys Maxwell should be used for 3D simulations.

D. PROPAGATION OF ESD CURRENT TO ONBOARD COMPONENTS

The ESD event identified in Section II-D and triggered when Eq. (4) is met, generates an electric current introduced from the contact point at the forearm link (see Figure 4 and 7) and propagated to the onboard electronic components through the elbow servo and the 4-wire cable along the upper arm link (Figure 3). This current results from the variation of charge when the electric potential of the aerial robot and the power line equalizes, as described in Eq. (1)-(2) [36]. As mentioned before, the complex distribution of the conductors (cables and metallic surfaces), insulating materials and other electronic components of the aerial robot makes difficult to analyze how the ESD current propagates to sensitive points of the system, in particular, the autopilot and electronic speed controllers. As described in [30]–[32], the ESD current will be indirectly coupled to the cables that connect the onboard components due to the inductive and radiated effects. The studies on ESD shielding with coaxial cables [38] show that the conductor of the shield could even facilitate the propagation of the ESD, so all parts of the system should be equally protected to the ESD. In practice, the electromagnetic susceptibility of the robot should be evaluated through ESD tests as described in [30] or in the IEEE Standard Techniques for High Voltage Testing.

E. MAGNETIC FIELD GENERATED BY THE POWER LINE

The presence of the magnetic field generated by the power line was identified in Figure 6 and Figure 8. According to [39], the magnetic flux density measured at a certain point of a three phase transmission line with no sag is given by:

$$\boldsymbol{B} = \begin{bmatrix} B_x \\ B_y \\ B_z \end{bmatrix} = \begin{bmatrix} B_a sin\,(\theta_a) + B_b sin\,(\theta_b) + B_c sin\,(\theta_c) \\ 0 \\ B_a cos\,(\theta_a) + B_b cos\,(\theta_b) + B_c cos\,(\theta_c) \end{bmatrix} \quad (6)$$

where B_a, B_b and B_c are the components of the magnetic field (in Tesla) generated by the current of the phases:

$$B_{(a,b,c)} = \frac{\mu_0 I_{(a,b,c)}}{2\pi r_{(a,b,c)}} \quad (7)$$

Here θ_a, θ_b, and θ_c are the angles of the corresponding rays with respect to the Z_{UAV} axis, as defined in Figure 11, μ_0 is the vacuum permeability, I is the current on each phase, and r is the distance to the sensor. Note that the Y-axis component of the magnetic field given by Eq. (6) is zero, in accordance with Figure 6 and Figure 8. Eq. (6) is useful for estimating the separation distance between the magnetometer and the power line so the magnetic interference is below a desired value [25].

According to the data logs shown in Figure 6, the magnetic field varies from −0.25 (robot landed) to −0.08 Gauss in the X-axis when the manipulator touches phase A, varying from 0.3 to 0.5 Gauss in the Z-axis. Thus, $B_x = 0.17$, $B_z = 0.2$ Gauss. In that moment $r_a = 0.6$, $r_b = 2$, $r_c = 4$ $[m]$, $\theta_a = 45$, $\theta_b = 80$, $\theta_c = 85[°]$ approximately. The nominal current in the line is around 100 [A], and with it, the magnetic field is

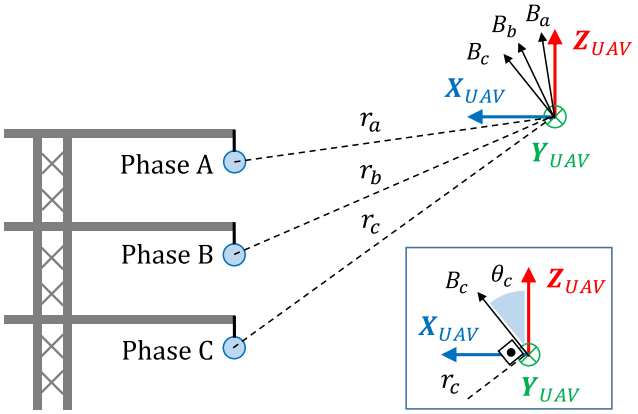

FIGURE 11. Components of the magnetic field generated by the power line, measured by the magnetometer of the multirotor (UAV).

$B \sim 0.3$ Gauss, according to Eq. (7). This is an estimation, as the real value depends on the current on the three phases.

IV. SHIELDED AND INSULATED CONFIGURATIONS

A. PRELIMINARY CONSIDERATIONS

The realization of inspection and maintenance operations on live power lines since the early 60's is carried out by the human operators using conductive suits [2], in such a way that the worker is inside a Faraday cage. The use of manned helicopters improved the maintenance of overhead lines in several ways. However, the proximity of the helicopter to the live line may cause the ESD between the cabin and people due to the effect of the electric field [17], resulting in an uncomfortable feeling for the operator. In order to identify the minimum distance at which the helicopter can be located without ESD occurring, experiments were carried out for a simplified model [16] and in a 500 kV line [17]. Depending on atmospheric conditions, the distance from which the ESD event could occur may vary. The IEEE Standard Techniques for High Voltage Testing (Std 4-1978) experimentally defines those minimum distances that must be respected so that there is no ESD. The IEEE Guide for maintenance methods on energized power lines (Std 516-2009) collected these values in a table (5 cm for 15 kV) [2].

The design of the protection mechanism for the aerial robot against the ESD produced by the transmission line should take into account the following considerations:

- The aerial robot is initially landed at zero potential. The platform must be discharged before it is manipulated by a person to avoid possible electric injuries due to the capacitive coupling (Equation (3)).
- The entry point of the ESD is the end effector or any point along the forearm link, as this will be the closest part of the aerial robot interacting with the power line.
- The electric charge tends to flow through those paths that present minor electric resistance, which depends on the dielectric strength of each medium. The minimum air insulation distance (MAID) for a 15 kV power line is 5 cm [2].

- The ESD will be indirectly coupled to the cables that connect the onboard components [30]–[32].
- The ESD current may generate interferences in the GHz band due to the radiated and induced fields [31], which may be absorbed by the wires acting as antennas [30].

Based on the antecedents and considerations mentioned above, the first solution to be evaluated consists of building a Faraday cage around the structure of the aerial manipulator.

B. SHIELDED AERIAL MANIPULATOR

Inspired on the conductive suits employed by the workers on the power lines [40], that act as Faraday cages, the first solution considered to protect the aerial manipulator from the electrostatic discharge was to cover the robotic arm and the multirotor with an adhesive copper paper, as shown in Figure 12. The idea is to facilitate the flow of the electric charge from the forearm link to the multirotor body, so it is distributed on the external surface without reaching the cables and electronic devices. The autopilot, ESC, Raspberry Pi, the connectors of the servos and all the cables were shielded with this material, connecting the devices to a common ground plane to avoid voltage differences. Additionally, the length of the wires was shortened as much as possible, removing loops to reduce the parasitic capacitance and inductance [30].

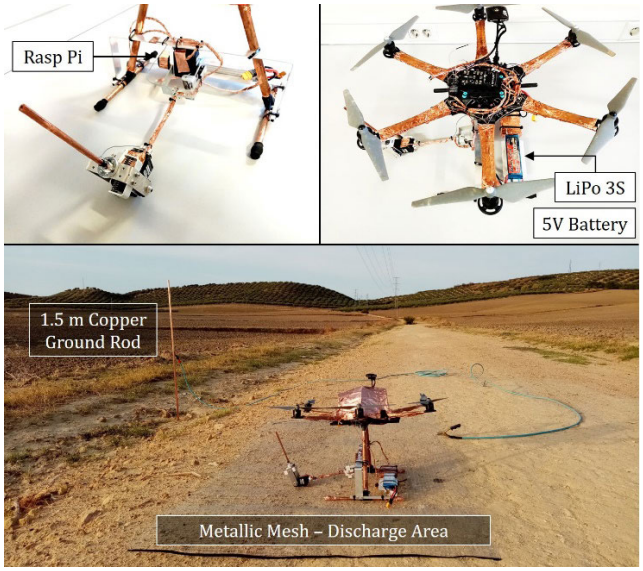

FIGURE 12. Shielded aerial manipulator and experimental setup.

Unlike drones like the DJI Phantom, which are completely closed by a fuselage, the frame structure of the S550 hexarotor is open, which complicates considerably the shield-ding, leaving some areas without cover or partially covered. This platform was preferred as it is widely used in research. Also shielding the cables properly is not an easy task, being another entry point for the ESD. In this sense, the study of the ESD entry through coaxial cable shields presented in [38] is illustrative. Since the charge capacity of the aerial robot increased with the added surface, it was deployed for safety reasons a metallic mesh connected to a copper ground rod for discharging the drone when it lands after touching the line (see Equation (3)).

The effectiveness of the shielding mechanism for the aerial manipulator was evaluated experimentally conducting Test 4 (see Table 1). Unfortunately, once again the six rotors stopped exactly when the arm touched the power line, causing a 360° flip in the pitch angle, as shown in the video attachment and in the image sequence depicted in Figure 13. This time, the aerial platform was able to recover the control before crashing, as the six propellers kept screwed on the motors. As mentioned in Section III-A, the crash in the experiment illustrated in Figure 7 was caused by the loss of one of the propellers due to the strong deceleration of the motors, as the visual inspection of the experiment suggested that the autopilot tried to recover the control one or two seconds after the contact. This hypothesis is confirmed with this experiment. Figure 14 shows the data log given by PX4, representing the multirotor position along with the norm of the magnetic field (which is especially useful to estimate the proximity of the multirotor to the power line), the angular rate, and the duty cycle of the PWM signal of the motors in the usual range 1 – 2 ms. The data log from the battery also shows a current drop from the nominal 22 [A] to 8 [A] in the two seconds interval when the motors are stopped. The interruption in the data log in Figure 8 was caused by the corruption of the log file due to the crash, as the operation conditions are similar in both cases.

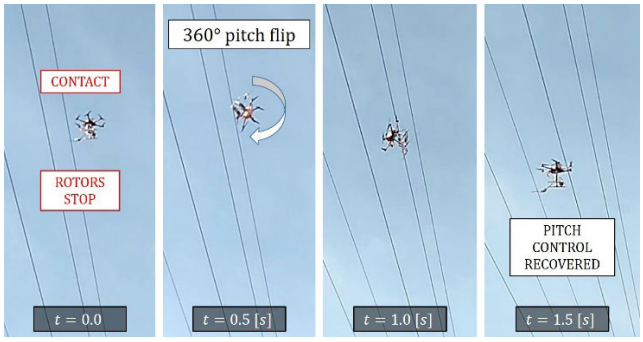

FIGURE 13. Sequence of images showing the 360° flip of the shielded aerial manipulator when the arm touches the power line.

As it can be seen in Figure 14, the failure occurs at t = 118 s, when the arm touches the line and the rotors stop. The autopilot reacts increasing the thrust until the actuators reach the saturation. Taking into account that the measurements of the angular rate and the PWM signals are coherent with the behavior of the platform, it is inferred that the ESD affected temporarily the electronic speed controllers of the brushless motors, as analyzed in Section III-A. The PX4 data log reports no problem on the RC signal, and no interruption was detected on the data log obtained from the Raspberry Pi. Although the robotic arm was set to a fixed

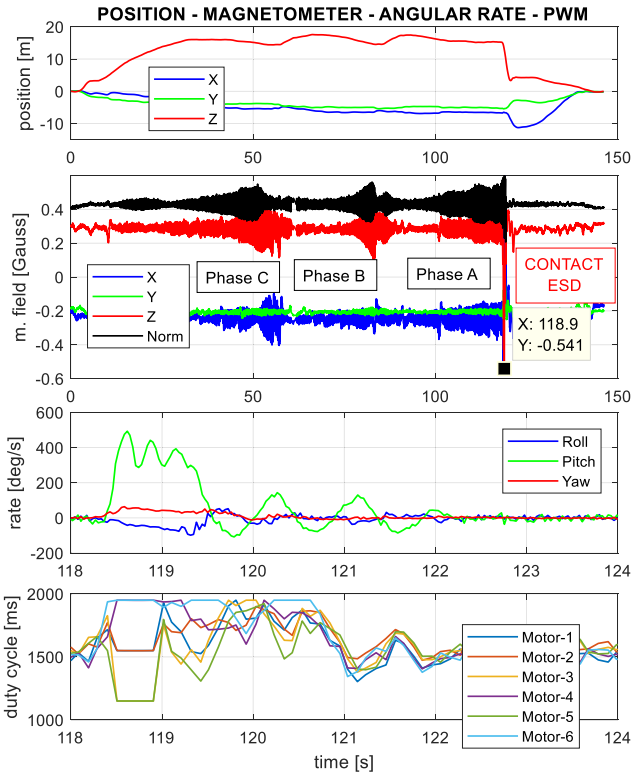

FIGURE 14. Multirotor position, magnetic field, angular rate and motors PWM given by PX4 during the experiment with the shielded aerial manipulator. Contact occurs at t = 118.6 s. The angular rate and duty cycle are represented for the interval when the aerial robot falls due to the ESD.

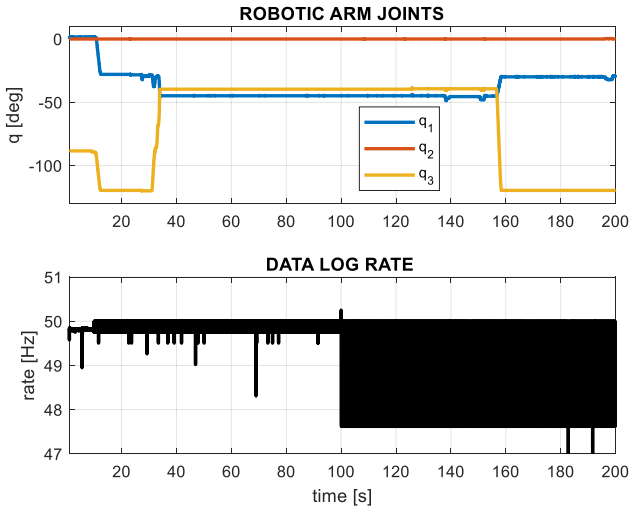

FIGURE 15. Data log of the robotic arm obtained from the Raspberry Pi 3B+ in the shielded aerial manipulator. The computer board and the autopilot have different time references since they are not connected.

position after the platform takes off, the rate in the data log and the measurements from the servos are continuous, as shown in Figure 15. As conclusion, and in accordance to [15] and [38], the imperfect shielding of the aerial platform did not protect properly the ESC, which seems to be the most sensitive component to the ESD.

C. LONG REACH AERIAL MANIPULATOR (INSULATED)

In anticipation of a possible failure in the shielded aerial manipulator, a second platform was developed and evaluated considering the opposite design principle: isolate electrically the manipulator from the aerial platform, introducing for this purpose a long reach PVC (polyvinyl chloride) link between both components. The prototype is shown in Figure 16. This is a variant of the long reach aerial manipulator presented in [8], employing a 500 × 18 × 2 mm PVC profile instead of the anodized aluminum profiles used in previous prototypes. The dielectric strength of this material is in the range 10 – 40 kV/mm, whereas the dielectric strength of the air is around 3 kV/mm. Thus, taking into account that the ESD will follow the path with the least electrical resistance (the air), the long reach link will isolate the multirotor for phase to ground voltages above 72 kV, as calculated in [2]. The length of the PVC link is determined empirically considering the lateral deflection [41] and the passive joint oscillation frequency [8], as well as the safety distance to prevent the collision with the power line.

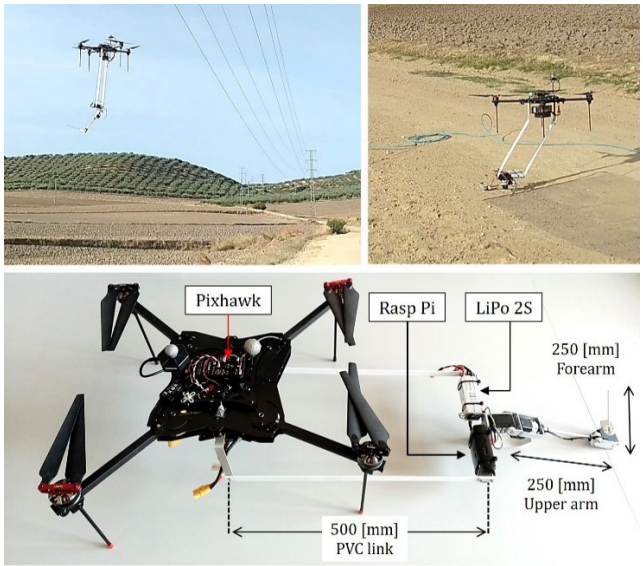

FIGURE 16. Long reach aerial manipulator with double PVC link (swing).

The aerial vehicle is a custom quadrotor built in carbon fiber, using T-motor MN3508 brushless motors with Multi-Pal 40A OPTO ESC (Simonk firmware), a Pixhawk v1 autopilot with PX4 v1.11.3, and a Taranis X9D radio. The platform is fed by a 6S 7000 mAh LiPo battery. The PVC links, separated 20 cm, are supported by a U-shaped aluminum frame attached to the quadrotor base, using polymer bearings to allow the free rotation of the pendulum joint. The manipulator is a 3-DOF robotic arm developed in [42], built with Herkulex DRS-0101 smart servos and a frame structure manufactured in anodized aluminum. The base of the manipulator is a 200 × 25 × 2 mm aluminum profile section that supports the 2S 1800 mAh LiPo battery, the Raspberry Pi 3B+, and the 5 V battery. A C-shaped

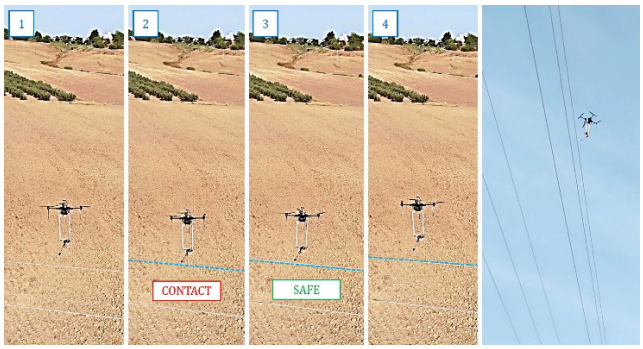

FIGURE 17. Sequence of images showing the safe interaction of the PVC long reach aerial manipulator with the 15 kV power line (first test).

aluminum frame is also attached at the base to protect the arm during the take-off and landing maneuvers. As it can be seen in Figure 16, there is no electrical connection between the arm and the multirotor, avoiding in this way the propagation of the electrostatic discharge. Figure 17 shows the safe interaction of this configuration with the power line in two consecutive tests [29]. The platform was controlled in position, while the arm is set to a nominal operation position. In order to implement a coordinated control scheme overcoming the disconnection between the manipulator and the multirotor, reference [43] proposes the implementation of a wireless communication link between both systems. The wrenches exerted by the long reach manipulator over the multirotor base can be also estimated measuring the rotation of the passive joint with an encoder [8] and the deflection of the link with a visual sensor as done in [41]. The experiment was repeated to validate the effectiveness of the insulation with the long reach configuration, showing in Figure 18 and 19 the corresponding sequence of images and data logs.

V. COMPARISON OF RESULTS

The in-flight contact experiments with the 15 kV live power line described in Sections II and IV, summarized in Table 2, evidence that the electronic speed controllers (ESC) of the drone can be severely affected by the electrostatic discharge, causing the sudden stop of the rotors and the potential crash of the platform. The electrical insulation of manipulator and multirotor is an effective solution to avoid this problem as long as the ESD current is not indirectly coupled through the wires and the electric field does not exceed the dielectric strength of the insulation material (3 kV/mm for air, 10 – 40 kV/mm for PVC). This is the case of the long reach aerial manipulator with PVC links (Section IV-C), which results particularly suitable to perform the installation of helical bird flight diverters due to the need for a large workspace to wrap the device on the power line, as illustrated in Figure 1. This configuration also reduces the risk of collision with the line and the noise introduced on the magnetometer, although the accuracy in the end effector positioning is reduced due to the oscillation on the long reach link.

The IEEE Guide for Maintenance Methods on Energized Power Lines [2] details the calculations and provides values for the minimum air insulation distance (MAID), that is, the shortest distance in the air between an energized electrical apparatus and the line worker at different potential: 5 cm for 15 kV, 11 cm for 30 kV, 24 cm for 60 kV, 28 cm for 72 kV. Note that these values correspond to the line-to-ground case (see Section 4.5.1 and Table D.1 in [2]), assuming that the aerial robot is at ground potential when approaching to the line. These values are useful for determining the minimum insulation distance between the manipulator and the multi-rotor to prevent the ESD and, consequently, the fault. The influence of this factor can be appreciated clearly comparing the results of experiments described in Section II. In the first case (II-C), the aluminum rod used

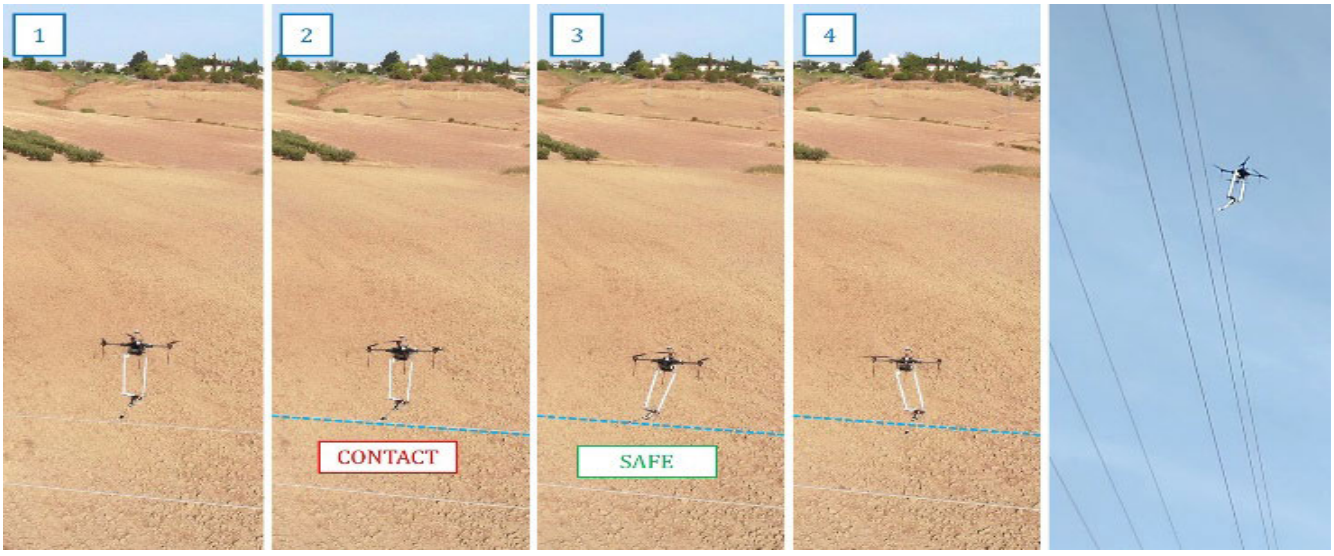

FIGURE 18. Sequence of images showing the safe interaction of the PVC long reach aerial manipulator with the 15 kV power line (second test).

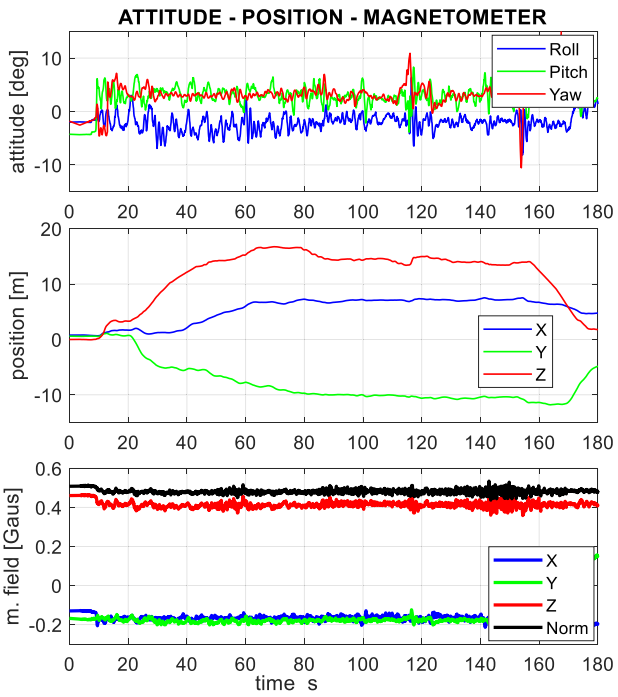

FIGURE 19. Multirotor attitude, position, and magnetic field in the long-reach configuration.

TABLE 2. Comparison of the experiments and related works.

Section	II-C	II-D	IV-B	IV-C
Aerial platform	Hexarotor	Hexarotor	Hexarotor	Quadrotor
ESC model	DJI 430 LITE	DJI 430 LITE	DJI 430 LITE	Multi-Pal 40A OPTO
Autopilot	Pixhawk	Pixhawk	Pixhawk	Pixhawk
Manipulator	Aluminum tube	Robotic arm 2-DOF	Robotic arm 2-DOF	Robotic arm 2-DOF
Anchor point	Landing gear leg	Multirotor base	Multirotor base	Long reach PVC link
Electrical protection	Insulated	None	Shielded	Insulated
Fault?	NO	YES: ESD	YES: ESD	NO
Fault result	-	Propeller out, crash	Free fall, recovered	-
Num. tests	2	1	1	3
Related works	[27][28]	[15][31] [32][44]	[14][27] [32][38]	[8][28][43]

to touch the power line and the onboard electronic components are electrically insulated by the leg of the landing gear, built with a 30 cm length carbon fiber tube covered by a non-conductive resin. In the second case (II-D), the electrical distance between the aluminum frame structure of the forearm link and the wires that connect the elbow joint servo with the rest of electronic components is less than 5 cm, causing the propagation of the ESD current to the ESC by indirect coupling, as described in [30]–[32].

Some technological solutions with drones have been recently shown performing the installation of clip-type bird diverters [27], [28] following opposite principles. In [27], the multirotor is directly exposed to the electrical interaction, whereas the system in [28] employs a long reach mechanism to insulate the platform. The design of electrical shields for multirotor platforms operating in high voltage power lines has not been properly documented so far. The LineDrone aerial robot presented in [14] employs an aluminum structure that also covers the onboard components, what increases considerably the weight (14 kg). Note that the mass density of carbon fiber and aluminum is 1.5 kg·cm^3 and 2.7 kg·cm^3, respectively. Thus, the use of aluminum to build a shielded frame structure reduces the effective payload capacity and operation time on flight. The test described in Section IV-B confirms that the imperfect shielding of the wires and on-board components does not protect the ESC from the ESD, but it may even facilitate its propagation, as stated in [38].

Electromagnetic simulation tools as the ones indicated in Section III-C can be applied to analyze the distribution of the electrostatic fields in aerial manipulation robots interacting in close range with high voltage power lines [14], [44], as well as in the design of shielding mechanisms [14], [27]. According to [16], [37], and as shown in Figure 10, the geometry of the robot influences the electric field in such a way that high electric potentials may arise in areas with high curvature, increasing the risk of ESD. The procedures described in [30] for evaluating the electromagnetic susceptibility of the on-board electronic components are also useful for identifying and preventing possible malfunctions of the aerial robot on flight, although it may be difficult in practice to reproduce the different effects that may occur on a real power line, what motivated the experimental approach followed in this work.

VI. CONCLUSION AND FUTURE WORK

Preliminary flight tests conducted on a real 15 kV power line revealed that the aerial manipulation robot is affected by the electrostatic discharge (ESD) induced when the robotic arm touches the line, causing a momentary malfunction in the electronic speed controllers and, consequently, the fall of the platform. Four platforms were evaluated: S550 platform with aluminum tube attached to the landing gear (safe interaction), S550 with 3-DOF robotic arm attached to the base (fault), shielded aerial manipulator (fault), and aerial manipulator with long reach PVC link (safe). The contact tests carried out with this configuration, in which the multirotor is electrically insulated from the aerial platform, show that the aerial robot is able to interact safely with the power line.

As future work, it is necessary to investigate the design of a reliable and effective shielding mechanism to protect the brushless motors and the electronic speed controllers from the electrostatic discharge. Additionally, it would be convenient to evaluate the susceptibility of a number of commercial ESCs to the ESD for voltages above 15 kV.

ACKNOWLEDGMENT

The authors would like to thank Jose Alberto Acosta, Jose Recacha, Jesus Zambrano, and Irene Martinez Diaz from ENDESA for facilitating the realization of the tests on the power lines.

REFERENCES

[1] (2020). *Secretaría de Estado de Energía, La energía en España, Ministerio Para la Transición Ecológica y el Reto Demográfico*. [Online]. Available: https://www.ree.es/es/actividades/gestor-de-la-red-y-transportista

[2] *IEEE Guide for Maintenance Methods on Energized Power Lines*, IEEE Standard 516-2009, Jun. 2009, pp. 1–144.

[3] F. Ruggiero, V. Lippiello, and A. Ollero, "Aerial manipulation: A literature review," *IEEE Robot. Autom. Lett.*, vol. 3, no. 3, pp. 1957–1964, Jul. 2018.

[4] M. Orsag, C. Korpela, P. Oh, and S. Bogdan, *Aerial Manipulation*. Cham, Switzerland: Springer-Verlag, 2018.

[5] A. Ollero, G. Heredia, A. Franchi, G. Antonelli, K. Kondak, A. Sanfeliu, A. Viguria, J. R. M.-D. Dios, F. Pierri, J. Cortes, A. Santamaria-Navarro, M. A. T. Soto, R. Balachandran, J. Andrade-Cetto, and A. Rodriguez, "The AEROARMS project: Aerial robots with advanced manipulation capabilities for inspection and maintenance," *IEEE Robot. Autom. Mag.*, vol. 25, no. 4, pp. 12–23, Dec. 2018.

[6] M. Trujillo, J. M.-D. Dios, C. Martín, A. Viguria, and A. Ollero, "Novel aerial manipulator for accurate and robust industrial NDT contact inspection: A new tool for the oil and gas inspection industry," *Sensors*, vol. 19, no. 6, p. 1305, Mar. 2019.

[7] T. Ikeda, S. Yasui, M. Fujihara, K. Ohara, S. Ashizawa, A. Ichikawa, A. Okino, T. Oomichi, and T. Fukuda, "Wall contact by octo-rotor UAV with one DoF manipulator for bridge inspection," in *Proc. IEEE/RSJ Int. Conf. Intell. Robots Syst. (IROS)*, Vancouver, BC, Canada, Sep. 2017, pp. 5122–5127.

[8] A. Suarez, F. Real, V. M. Vega, G. Heredia, A. Rodriguez-Castaño, and A. Ollero, "Compliant bimanual aerial manipulation: Standard and long reach configurations," *IEEE Access*, vol. 8, pp. 88844–88865, 2020.

[9] S. Hamaza, I. Georgilas, M. Fernandez, P. Sanchez, T. Richardson, G. Heredia, and A. Ollero, "Sensor installation and retrieval operations using an unmanned aerial manipulator," *IEEE Robot. Autom. Lett.*, vol. 4, no. 3, pp. 2793–2800, Jul. 2019.

[10] M. Tognon, H. A. T. Chavez, E. Gasparin, Q. Sable, D. Bicego, A. Mallet, M. Lany, G. Santi, B. Revaz, J. Cortes, and A. Franchi, "A truly-redundant aerial manipulator system with application to push-and-slide inspection in industrial plants," *IEEE Robot. Autom. Lett.*, vol. 4, no. 2, pp. 1846–1851, Apr. 2019.

[11] H. W. Wopereis, M. Fumagalli, W. L. W. van de Ridder, T. J. W. Lankhorst, L. Klooster, E. M. Bukai, D. Wuthier, G. Nikolakopoulos, S. Stramigioli, and J. B. C. Engelen, "Multimodal aerial locomotion: An approach to active tool handling," *IEEE Robot. Autom. Mag.*, vol. 25, no. 4, pp. 57–65, Dec. 2018.

[12] H. Paul, R. Miyazaki, R. Ladig, and K. Shimonomura, "Landing of a multirotor aerial vehicle on an uneven surface using multiple on-board manipulators," in *Proc. IEEE/RSJ Int. Conf. Intell. Robots Syst. (IROS)*, Macau, China, Nov. 2019, pp. 1926–1933.

[13] *AERIAL-CORE Project Homepage*. Accessed: Jul. 1, 2021. [Online]. Available: https://aerial-core.eu/

[14] F. Miralles, P. Hamelin, G. Lambert, S. Lavoie, N. Pouliot, M. Montfrond, and S. Montambault, "LineDrone technology: Landing an unmanned aerial vehicle on a power line," in *Proc. IEEE Int. Conf. Robot. Autom. (ICRA)*, Brisbane, QLD, Australia, May 2018, pp. 6545–6552.

[15] M. Heggo, K. Kabbabe, V. Peesapati, R. Gardner, S. Watson, and W. Crowther, "Operation of aerial inspections vehicles in HVDC environments part A: Evaluation and Mitigation of high electrostatic field impact," *J. Phys., Conf. Ser.*, vol. 1356, Oct. 2019, Art. no. 012009.

[16] D. Yu, S. Wan, F. Chen, X. Bian, L. Chen, M. MacAlpine, J. Zhang, L. Zhang, and L. Wang, "The effect of floating-potential conductors on the electric field near overhead transmission lines," *J. Electrostatics*, vol. 70, no. 3, pp. 339–345, Jun. 2012.

[17] S. Wan, X. Bian, L. Chen, D. Yu, L. Wang, and Z. Guan, "Electrostatic discharge effect on safe distance determination for 500 kV AC power line's helicopter inspection," *J. Electrostatics*, vol. 71, no. 4, pp. 778–780, Aug. 2013.

[18] A. Suarez, A. E. Jimenez-Cano, V. M. Vega, G. Heredia, A. Rodriguez-Castaño, and A. Ollero, "Design of a lightweight dual arm system for aerial manipulation," *Mechatronics*, vol. 50, pp. 30–44, Apr. 2018.

[19] G. Garimella and M. Kobilarov, "Towards model-predictive control for aerial pick-and-place," in *Proc. IEEE Int. Conf. Robot. Autom. (ICRA)*, Seattle, WA, USA, May 2015, pp. 4692–4697.

[20] A. Suarez, V. M. Vega, M. Fernandez, G. Heredia, and A. Ollero, "Benchmarks for aerial manipulation," *IEEE Robot. Autom. Lett.*, vol. 5, no. 2, pp. 2650–2657, Apr. 2020.

[21] A. B. Alhassan, X. Zhang, H. Shen, and H. Xu, "Power transmission line inspection robots: A review, trends and challenges for future research," *Int. J. Electr. Power Energy Syst.*, vol. 118, Jun. 2020, Art. no. 105862.

[22] L. Yang, J. Fan, Y. Liu, E. Li, J. Peng, and Z. Liang, "A review on state-of-the-art power line inspection techniques," *IEEE Trans. Instrum. Meas.*, vol. 69, no. 12, pp. 9350–9365, Dec. 2020.

[23] S. Hrabar, T. Merz, and D. Frousheger, "Development of an autonomous helicopter for aerial powerline inspections," in *Proc. 1st Int. Conf. Appl. Robot. Power Ind.*, Oct. 2010, pp. 1–6.

[24] T. He, Y. Zeng, and Z. Hu, "Research of multi-rotor UAVs detailed autonomous inspection technology of transmission lines based on route planning," *IEEE Access*, vol. 7, pp. 114955–114965, 2019.

[25] D. Martinović, S. Bogdan, and Z. Kovačić, "Mathematical considerations for unmanned aerial vehicle navigation in the magnetic field of two parallel transmission lines," *Appl. Sci.*, vol. 11, no. 8, p. 3323, Apr. 2021.

[26] A. Suarez, P. J. Sanchez-Cuevas, G. Heredia, and A. Ollero, "Aerial physical interaction in grabbing conditions with lightweight and compliant dual arms," *Appl. Sci.*, vol. 10, no. 24, p. 8927, Dec. 2020.

[27] *UAV Installation Services—Bird Diverters*. Accessed: Jun. 6, 2021. [Online]. Available: https://www.youtube.com/watch?v=PfkRt2W7NAk

[28] *Crocfast Bird Diverter Installation by Drone*. Accessed: Jun. 6, 2021. [Online]. Available: https://www.youtube.com/watch?v=qGwk8VMFp0M

[29] *Video of the Experiments*. Accessed: Jun. 6, 2021. [Online]. Available: https://www.youtube.com/watch?v=IO8gHE0CfNs

[30] "EMC design guide for STM8, STM32 and legacy MCUs," ST Microelectron., Geneva, Switzerland, Appl. Note AN1709, 2018.

[31] O. Fujiwara, "An analytical approach to model indirect effect caused by electrostatic discharge," *IEICE Trans. Commun.*, vol. 79, no. 4, pp. 483–489, 1996.

[32] G. Cerri, R. D. Leo, and V. M. Primiani, "ESD indirect coupling modeling," *IEEE Trans. Electromagn. Compat.*, vol. 38, no. 3, pp. 274–281, Aug. 1996.

[33] J. Tranen and G. Wilson, "Electrostatically induced voltages and currents on conducting objects under EHV transmission lines," *IEEE Trans. Power App. Syst.*, vol. PAS-90, no. 2, pp. 768–776, Mar. 1971.

[34] D. W. Deno, "Currents induced in the human body by high voltage transmission line electric field measurement and calculation of distribution and dose," *IEEE Trans. Power App. Syst.*, vol. PAS-96, no. 5, pp. 1517–1527, Sep. 1977.

[35] R. G. Olsen and J. T. Leman, "On calculating contact current for objects insulated from the earth and immersed in quasi-static electric fields," *IEEE Power Energy Technol. Syst. J.*, vol. 4, no. 1, pp. 16–23, Mar. 2017.

[36] W. D. Greason, "Generalized model of electrostatic discharge (ESD) for bodies in approach: Analyses of multiple discharges and speed of approach," *J. Electrostatics*, vol. 54, no. 1, pp. 23–37, Jan. 2002.

[37] L. Dascalescu, P. Ribardiere, J.-M. Paillot, and R. Allam, "Computational estimation of ESD conditions between a charged body and a conductor of floating potential," *IEEE Trans. Ind. Appl.*, vol. 37, no. 3, pp. 759–765, May/Jun. 2001.

[38] S. Van den Berghe and D. De Zutter, "Study of ESD signal entry through coaxial cable shields," *J. Electrostatics*, vol. 44, nos. 3–4, pp. 135–148, Sep. 1998.

[39] Q. Huang, W. Zhen, and P. W. T. Pong, "A novel approach for fault location of overhead transmission line with noncontact magnetic-field measurement," *IEEE Trans. Power Del.*, vol. 27, no. 3, pp. 1186–1195, Jul. 2012.

[40] P. W. Hotte, G. Gela, J. D. Mitchell, and P. F. Lyons, "Electrical performance of conductive suits," *IEEE Trans. Power Del.*, vol. 12, no. 3, pp. 1193–1201, Jul. 1997.

[41] A. Suarez, A. M. Giordano, K. Kondak, G. Heredia, and A. Ollero, "Flexible link long reach manipulator with lightweight dual arm: Soft-collision detection, reaction, and obstacle localization," in *Proc. IEEE Int. Conf. Soft Robot. (RoboSoft)*, Livorno, Italy, Apr. 2018, pp. 406–411.

[42] A. Suarez, A. Caballero, A. Garofano, P. J. Sanchez-Cuevas, G. Heredia, and A. Ollero, "Aerial manipulator with rolling base for inspection of pipe arrays," *IEEE Access*, vol. 8, pp. 162516–162532, 2020.
[43] R. Miyazaki, H. Paul, T. Kominami, and K. Shimonomura, "Wire-suspended device control based on wireless communication with multirotor for long reach-aerial manipulation," *IEEE Access*, vol. 8, pp. 172096–172104, 2020.
[44] N. Iversen, A. Kramberger, O. B. Schofield, and E. Ebeid, "Pneumatic-mechanical systems in UAVs: Autonomous power line sensor unit deployments," in *Proc. IEEE Int. Conf. Robot. Automat.*, Feb. 2021.

ALEJANDRO SUAREZ received the degree in telecommunication engineering and the M.Sc. degree in automation and robotics from the University of Seville, Spain, in 2012 and 2014, respectively, and the Ph.D. degree in robotics in 2019. Since 2012, he has been with the Robotics, Vision and Control Group, working in the FP7 EC-SAFEMOBIL Project, and the PERIGEO and CLEAR Spanish projects. In 2014, he obtained a FPU Grant from the Spanish Ministry of Education, Culture and Sport for supporting his research activity as a Ph.D. student in the frame of the AEROARMS H2020 Project. During three months he stayed at the Robotics and Mechatronics Institute, DLR, Oberpfaffenhofen. He is currently working on the AERIAL-CORE H2020 Project and the ERC Advanced GRIFFIN Project. He is author of more than 30 articles in international conferences and journals. His research interests include humanoid robots and the development of anthropomorphic, compliant and lightweight robotic arms (LiCAS).

RAFAEL SALMORAL was born in Cordoba, Spain. He is currently an Aerospace Engineer with the University of Seville, combining his work for the Robotics, Vision and Control Group (GRVC) as a Research and Development Engineer and Experimental RPA Pilot with the direction of his engineering company Proskytec Research & Engineering. His research interests include hybrid fixed wing-VTOL platforms and the use of virtual reality and augmented reality for robot remote operation.

PEDRO J. ZARCO-PERIÑAN was born in Seville, Spain. He received the Ph.D. degree in electrical engineering from the University of Seville and the M.B.A. degree from Deusto University. Since 1989, he has been with the Department of Electrical Engineering, University of Seville, where he is currently an Assistant Professor. He has worked in different electricity companies. His research interests include the development and maintenance of facilities, optimization of energy systems, and power system planning. He has been a member of technical committees for the development of standards and regulations for the Spanish electricity sector.

ANIBAL OLLERO (Fellow, IEEE) is currently a Full Professor, the Head of the GRVC Robotics Laboratory, University of Seville, and a Scientific Advisor of the Center for Advanced Aerospace Technologies (CATEC), Seville, Spain. He has been a Full Professor with the Universities of Santiago and Malaga, Spain, a Researcher with the Robotics Institute of Carnegie Mellon University, Pittsburgh, USA, and LAAS-CNRS, Toulouse, France. He has authored more than 750 publications, including nine books, 200 journal articles, led about 160 projects, and transferring results to many companies. He has supervised 43 Ph.D. thesis. He has participated in 25 European Projects being a Coordinator of five, including the FP7-EC integrated projects ARCAS and ECSAFEMOBIL, and the current H2020 AEROARMS. He was a member of the Board of Directors of euRobotics, until March 2019. He is IEEE Fellow for his contributions to the development and deployment of aerial robots. He was a recipient of 14 awards. He is the Co-Chair of the IEEE Technical Committee on Aerial Robotics and Unmanned Aerial Vehicles. He is the Coordinator of the Aerial Robotics Topic Group de euRobotics. He has been a Founder and the President of the Spanish Society for the Research and Development in Robotics (SEIDROB) until November 2017.